

One step model of photo-emission at finite temperatures: spin fluctuations of Fe(001)

Ján Minár

*New Technologies-Research Center, University of West Bohemia,
Univerzitní 8, 306 14 Plzeň, Czech Republic.**

Sergey Mankovsky, Jürgen Braun, and Hubert Ebert

*Department of Chemistry, LMU Munich,
Butenandtstraße 11, 81377 München, Germany.*

(Dated: March 1, 2022)

Abstract

Various technical developments extended the potential of angle-resolved photoemission (ARPES) tremendously during the last twenty years. In particular improved momentum, energy and spin resolution as well as the use of photon energies from few eV up to several keV makes ARPES a rather unique tool to investigate the electronic properties of solids and surfaces. With our work we present a generalization of the state of the art description of the photoemission process, the so called one-step model that describes excitation, transport to the surface and escape into the vacuum in a coherent way. In particular, we present a theoretical description of temperature-dependent ARPES with a special emphasis on spin fluctuations. Finite temperature effects are included within the so called alloy analogy model which is based on the coherent potential approximation and this way allows to describe uncorrelated lattice vibrations in combination with spin fluctuations quantitatively on the same level of accuracy. To demonstrate the applicability of our approach a corresponding numerical analysis has been applied to spin- and angle-resolved photoemission of Fe(100) at finite temperatures.

I. INTRODUCTION

The experimental and theoretical studies on itinerant electron ferromagnetism address one of the crucial problems in condensed matter physics (for reviews, see Ref. 1). One of the most important experimental tools to get direct insight into the electronic structure of solids and surfaces is angle-resolved photoemission spectroscopy (ARPES). In particular, spin- and angle-resolved photoemission (SARPES) has been developed into a powerful method to study surface and thin film magnetism². Very recently this technique has been used extensively to investigate the topological properties of solid state materials³. In the 1980-ies first experimental studies using SARPES had been devoted to probe the existence of local magnetic moments at temperatures close and above the Curie temperature T_C . Pioneering SARPES experiments had been performed in particular by Kisker et al.⁴⁻⁶ on Fe(001). At that time two contrary models had been proposed to describe the ferromagnetic to paramagnetic transition at the critical temperature. On the one-hand side, the so-called Stoner model proposed the breakdown of the exchange splitting of bands leading this way to the non-magnetic phase. On the other hand the existence of local fluctuating magnetic moments above the Curie temperature according to the Heisenberg model was suggested. SARPES studies on magnetic transition metals (Fe and Co) were able to clearly identify the exchange-split bands at lower temperatures and fluctuating moments at high temperatures².

Unfortunately, after the pioneering SARPES experiments at elevated temperatures, most of the more recent SARPES studies were done at room or even at very low temperatures for a variety of materials including superconductors, topological materials etc.^{3,7,8}. The main reason for this is found in a possible contamination of the electron analyzer and UHV chamber after heating of the thin film samples which leads to a significant decrease of the pressure in the UHV chamber. However, the thermal vibrations in combination with spin fluctuations turned out to be a very important issue for photoemission spectra measured at high photon energy ranging from soft to hard-X-rays⁹⁻¹³. Going to higher photon energies has the advantage of a longer inelastic mean free path of the photoelectrons and turns ARPES to a bulk sensitive technique. However, higher photon energies challenge the interpretation of the corresponding experimental spectra. In particular, even at very low temperatures (tenths of a Kelvin), indirect transitions occur which in consequence lead to the XPS limit. The corresponding averaging over the Brillouin zone leads to density of states like spectra

for any emission angle and the access to the ground state band structure is lost¹⁴. Finally, spin fluctuations play an important role in the description of ultrafast processes measured by pump-probe angle-resolved photoemission and two photon photoemission spectroscopy. Absorption of a very intense pump-pulse leads in the first femtoseconds to the increase of the electronic temperature and after several hundreds of femtoseconds the energy is dissipated into the lattice. Very recently, first time-dependent SARPES measurements have been performed for topological insulators¹⁵. Furthermore, Eich et al. performed a detailed study on possible ultrafast demagnetization processes in ferromagnetic transition metals by SARPES¹⁶.

It is well known that density functional theory (DFT) in its local spin-density approximation is able to describe quantitatively the ground state and magnetic properties of transition metals at $T = 0$ K. This rigorous description can be extended also to finite temperatures. The most common multi-scale approach in this direction is based on the calculation of the so called exchange coupling constants¹⁷ for a classical Heisenberg model on the basis of DFT and to perform subsequent Monte Carlo or spin dynamics simulations. On the other hand, it has been realized since many years that locally fluctuating magnetic moments are a consequence of local electronic correlations. A very successful method to go beyond the DFT-LSDA scheme is the dynamical mean field theory (DMFT) in combination with DFT. Liechtenstein et al. showed that such a DFT+DMFT approach can quantitatively describe temperature-dependent magnetism in Fe and Ni¹⁸. However such an approach does not take into account lattice vibrations which are present at all finite temperatures. On the other hand, a scheme to deal with thermal lattice vibrations is provided by the so-called alloy analogy model¹⁹ that takes the necessary thermal average by means of the coherent potential approximation (CPA) alloy theory. This approach was already applied successfully to deal with ARPES of non-magnetic materials at finite temperatures²⁰. In addition, following the original idea behind the alloy analogy model it was extended to account for thermally induced spin fluctuations in magnetic materials²¹ as well. This opens the combination with various models to deal with thermal spin fluctuations as for example the disordered local moment approach^{22,23}. Another advantage of the approach is its possible combination with methods describing local correlations as for example LSDA+U and LSDA+DMFT. This was demonstrated recently for Gd, where temperature dependence of the longitudinal resistivity and the anomalous Hall effect was studied²⁴.

It is widely accepted to interpret a measured photoelectron spectrum by referring to the results of band-structure calculations. Such an interpretation is questionable for moderately and even more for strongly correlated systems. On the other hand, the most reliable theoretical approach to interpret ARPES spectra is provided by the so-called one-step model of photoemission. This approach was formulated first by Pendry and co-workers^{25,26} in the framework of multiple scattering theory and has been recently generalized to include various aspects like e.g. disorder, lattice vibrations, electronic correlations, the fully relativistic spin-density matrix formulation and time-dependent pump-probe aspects^{8,27,28}. However this scheme did not allow up to now to consider temperature-dependent spin fluctuations in combination with lattice vibrations. In this paper we generalize the one-step model of photoemission in order to include spin-fluctuations and lattice vibrations on the same level of accuracy within the framework of the alloy analogy model.

The paper is organized as follows: In Sec. II we describe the theoretical approach, the so called alloy analogy model, which has been applied to the one-step model of photoemission in the framework of the SPR-KKR method. In Secs. IV A and IV B we apply this formalism and calculate temperature-dependent, spin-polarized ARPES spectra for Fe(001). In Sec. V we summarize our results.

II. THEORETICAL APPROACH: THERMAL EFFECTS

Considering the electronic structure of a magnetic solid at finite temperature, its modification due to thermal lattice and magnetic excitations has to be taken into account. The present approach is based on the adiabatic treatment of the non-correlated localized thermal displacements of atoms from their equilibrium positions (thermal lattice vibrations) in combination with a tilt of the local magnetic moments away from their orientation in the ground state (thermal spin fluctuations). Multiple scattering theory allows to describe uncorrelated local thermal vibrations and spin fluctuations within the single-site CPA alloy theory. This implies the reduction of the calculation of a thermal average to the calculation of the configurational average in complete analogy to the averaging for random, substitutional alloy systems. The impact of thermal effects on the electronic structure, taken into account within such an approach, was discussed previously in order to describe the temperature dependent transport properties and Gilbert damping in magnetic systems²⁸. The

impact of the thermal lattice vibrations was also studied in calculations of temperature-dependent photoemission of non-magnetic systems²⁰, however the inclusion of the thermal spin fluctuations for ferromagnetic systems is missing and in the following we generalize the one-step model of photoemission accordingly.

A. Alloy analogy model

Within the alloy analogy model, lattice vibrations are described by a discrete set of N_v displacement vectors $\Delta\vec{R}_v^q(T)$ for each atom in the unit cell. The temperature dependent amplitude of the displacements is taken to be equal to the root mean square displacement $(\langle u^2 \rangle_T)^{1/2}$, $|\Delta\vec{R}_v^q(T)| = \langle u_q^2 \rangle_T^{1/2}$, with the probabilities $x_v = 1/N_v$ ($v = 1, \dots, N_v$). $[\langle u_q^2 \rangle_T]^{1/2}$ is evaluated here within the Debye model with the Debye temperature Θ_D taken from experiment.

Using the rigid muffin-tin approximation^{29,30}, the displaced atomic potential is associated with a corresponding single-site t-matrix \underline{t} that has to be referred with respect to the common global frame of reference. This quantity is obtained by a coordinate transformation from local single-site t-matrix $\underline{t}^{\text{loc}}$ via the expression:

$$\underline{t} = \underline{U}(\Delta\vec{R}) \underline{t}^{\text{loc}} \underline{U}(\Delta\vec{R})^{-1}. \quad (1)$$

In the following the underline symbol represents a matrix in the angular momentum representation. In the fully relativistic formulation case, as adopted here, this implies a labelling of the matrix elements with the relativistic quantum numbers $\Lambda = \kappa, \mu$ ³¹. The so-called U-transformation matrix $\underline{U}(\vec{s})$ in Eq. (1) is given in its non-relativistic form by:^{29,30}

$$U_{LL'}(\vec{s}) = 4\pi \sum_{L''} i^{l+l''-l'} C_{LL'L''} j_{l''}(|\vec{s}|k) Y_{L''}(\hat{s}). \quad (2)$$

Here $L = (l, m)$ represents the non-relativistic angular momentum quantum numbers, $j_l(x)$ is a spherical Bessel function, $Y_L(\hat{r})$ a real spherical harmonics, $C_{LL'L''}$ a corresponding Gaunt number and $k = \sqrt{E}$ is the electronic wave vector. The relativistic version of the U-matrix is obtained by a standard Clebsch-Gordan transformation.³¹

To account for the impact of disorder caused by thermal spin fluctuations, the continuous distribution $P(\hat{e})$ for the orientation of local magnetic moments is replaced by a discrete set of orientation vectors \hat{e}_f (with $f = 1, \dots, N_f$) occurring with a probability x_f . The

configurational average for this discrete set of orientations is made using the CPA leading to a periodic effective medium.

The rigid spin approximation¹⁷ used in the calculations implies that the spin-dependent part B_{xc} of the exchange-correlation potential does not change for the local frame of reference fixed to the magnetic moment when the moment is oriented along an orientation vector \hat{e}_f . As a result, the single-site t-matrix $\underline{t}_f^{\text{loc}}$ considered in the local frame is the same for all orientation vectors. With respect to the common global frame that is used to deal with the multiple scattering problem (see Eq. (8)) the t-matrix for a given orientation vector (\hat{e}_f) is determined by:

$$\underline{t}_f = \underline{R}(\hat{e}_f) \underline{t}^{\text{loc}} \underline{R}(\hat{e}_f)^{-1} , \quad (3)$$

with the transformation from the local to the global frame of reference expressed by the rotation matrices $\underline{R}_f = \underline{R}(\hat{e}_f)$.³¹ The temperature dependent probability $x_f = x(\hat{e}_f)$ for each orientation \hat{e}_f and an appropriate Weiss field parameter $w(T)$ is given by the expression³²:

$$x_f = \frac{\exp(-w(T)\hat{e}_z \cdot \hat{e}_f/kT)}{\sum_{f'} \exp(-w(T)\hat{e}_z \cdot \hat{e}_{f'}/kT)} . \quad (4)$$

The various types of disorder discussed above may be combined with each other as well as with chemical i.e. substitutional disorder. In the most general case a pseudo-component (vft) is characterized by its chemical atomic type t , the spin fluctuation f and lattice displacement v . Using the rigid muffin-tin and rigid spin approximations, the single-site t-matrix $\underline{t}_t^{\text{loc}}$ in the local frame is independent from the orientation vector \hat{e}_f and displacement vector $\Delta\vec{R}_v$, and coincides with \underline{t}_t for the atomic type t . With respect to the common global frame one has accordingly the t-matrix:

$$\underline{t}_{vft} = \underline{U}(\Delta\vec{R}_v) \underline{R}(\hat{e}_f) \underline{t}_t \underline{R}(\hat{e}_f)^{-1} \underline{U}(\Delta\vec{R}_v)^{-1} . \quad (5)$$

With this the resulting CPA equations are identical to the standard CPA Eqs. (6) to (8) below with the index t identifying atom types replaced by the combined index (vft). The corresponding pseudo-concentration x_{vft} combines the concentration x_t of the atomic type t with the probability for the orientation vector \hat{e}_f and displacement vector $\Delta\vec{R}_v$. This leads to the site diagonal configurational average which can be determined by solving the

multi-component CPA equations³³:

$$\underline{\mathcal{I}}_{\text{CPA}} = \sum_t x_t \underline{\mathcal{I}}_{vft} \quad (6)$$

$$\underline{\mathcal{I}}_t = [(\underline{t}_{vft})^{-1} - (\underline{t}_{\text{CPA}})^{-1} + (\underline{\mathcal{I}}_{\text{CPA}})^{-1}]^{-1} \quad (7)$$

$$\underline{\mathcal{I}}_{\text{CPA}} = \frac{1}{\Omega_{\text{BZ}}} \int_{\Omega_{\text{BZ}}} d^3k \left[(\underline{t}_{\text{CPA}})^{-1} - \underline{G}(\vec{k}, E) \right]^{-1}, \quad (8)$$

where again the underline symbol indicates matrices with respect to the combined index Λ .

B. One step model of ARPES

The main idea of the one-step model of photoemission is to describe the excitation process, the transport of the photoelectron to the surface as well as the escape into the vacuum in a coherent way as a single quantum mechanical process²⁵. The one-step model of ARPES is based on the Fermi's golden rule and was originally implemented for ordered surfaces using the multiple scattering KKR formalism (for more details see review in Ref. 34). This approach has been generalized to describe photoemission of disordered alloys by means of the CPA^{35,36}. Recently it was extended to deal with thermal lattice vibration effects exploiting the alloy analogy model described above. This approach was successfully applied to describe indirect transitions which occur in soft- and hard-X-ray photoemission²⁰. Based on the CPA approach the temperature-dependent spin-density matrix ρ for a given kinetic energy ϵ_f and wave vector \mathbf{k}_{\parallel} can be written in the following form:

$$\begin{aligned} \langle \bar{\rho}_{ss'}(\epsilon_f, \mathbf{k}_{\parallel}, T) \rangle \propto & \langle \bar{\rho}_{ss'}^{at}(\epsilon_f, \mathbf{k}_{\parallel}, T) \rangle + \langle \bar{\rho}_{ss'}^c(\epsilon_f, \mathbf{k}_{\parallel}, T) \rangle \\ & + \langle \bar{\rho}_{ss'}^{inc}(\epsilon_f, \mathbf{k}_{\parallel}, T) \rangle + \langle \bar{\rho}_{ss'}^{surf}(\epsilon_f, \mathbf{k}_{\parallel}, T) \rangle, \end{aligned} \quad (9)$$

with a purely atomic part (*at*), a coherent part (*c*) with multiple scattering involved and an incoherent (*inc*) part as described in detail in Refs. 37 and 38 in the context of chemical disorder in alloys. The third, incoherent contribution which appears due to the CPA-averaging procedure represents an on-site quantity that behaves DOS-like³⁷. The last contribution is the surface (*surf*) part of the spin-density matrix. As dispersing and non-dispersing contributions are clearly distinguishable we can define the spin-density matrix which describes the angle-integrated (AIPES) photoemission

$$\langle \bar{\rho}_{ss'}^{\text{AIPES}}(\epsilon_f, \mathbf{k}_{\parallel}, T) \rangle \sim \langle \bar{\rho}_{ss'}^{at}(\epsilon_f, \mathbf{k}_{\parallel}, T) \rangle + \langle \bar{\rho}_{ss'}^{inc}(\epsilon_f, \mathbf{k}_{\parallel}, T) \rangle + \langle \bar{\rho}_{ss'}^{surf}(\epsilon_f, \mathbf{k}_{\parallel}, T) \rangle, \quad (10)$$

where the \mathbf{k} -dependence in the atomic and incoherent contributions is only due to the final state. A \mathbf{k} -averaging is not necessary because the \mathbf{k} -dependence of the (SP)LEED-type final state is very weak and can be neglected in explicit calculations. Furthermore, when using the single-scatterer approximation for the final state the \mathbf{k} -dependence completely vanishes. This way a direct comparison to corresponding measurements is given in both cases.

In terms of the spin-density matrix ρ the intensity of the photocurrent can be written as:

$$I(\epsilon_f, \mathbf{k}_{\parallel}, T) = \text{Tr} \left(\rho_{ss'}(\epsilon_f, \mathbf{k}_{\parallel}, T) \right) , \quad (11)$$

with the corresponding spin polarization vector given by:

$$\mathbf{P} = \frac{1}{I} \text{Tr} \left(\boldsymbol{\sigma} \rho \right) . \quad (12)$$

Finally, the spin-projected photocurrent is obtained from the following expression:

$$I_{\mathbf{n}}^{\pm} = \frac{1}{2} \left(1 \pm \mathbf{n} \cdot \mathbf{P} \right) , \quad (13)$$

with the spin polarization (\pm) referring to the vector \mathbf{n} .

Within our approach, we aim on a generalized spin-density matrix formalism for the photocurrent to include spin fluctuations and thermal vibrations on the same level of accuracy. The formalism presented in section II A provides us with the temperature-dependent single-site scattering matrix \underline{t}_{vft} which enters the multiple scattering KKR formalism to calculate the photocurrent $I(\epsilon_f, \mathbf{k}_{\parallel}, T)$. (A detailed description of the generalized fully relativistic one-step model for disordered magnetic alloys can be found in Ref. 8). Special care has to be taken concerning the temperature-dependent averaging of the photoemission matrix elements, in contrast to the previous work which did not account for spin fluctuations²⁰. Within the above mentioned rigid spin approximation³⁹, the regular $\underline{M}_{i'}^{\text{loc}}$ and irregular $\underline{I}_{i',j'}^{\text{loc}}$ dipole matrix transition elements are first calculated for the local frame of reference fixed to the magnetic moment when the moment is oriented along an orientation vector \hat{e}_f with the components i' and j' of the light polarization vector referred to the local frame of reference (x', y', z') with $\hat{e}_{z'} = \hat{e}_f$. In the case of spin fluctuations, the transformation of the matrix elements into the global frame of reference includes also a rotation of the polarization. For the regular matrix elements one finds:

$$\underline{M}_i^{\text{vft}} = \sum_{i'} D_{ii'}(\hat{e}_f) \underline{U}(\Delta \vec{R}_v) \underline{R}(\hat{e}_f) \underline{M}_{i'}^{\text{loc}} \underline{R}(\hat{e}_f)^{-1} \underline{U}(\Delta \vec{R}_v)^{-1} , \quad (14)$$

and for the irregular matrix elements one has accordingly:

$$\underline{I}_{ij}^{\text{vft}} = \sum_{i'j'} D_{ii'}(\hat{e}_f) D_{jj'}(\hat{e}_f) \underline{U}(\Delta\vec{R}_v) \underline{R}(\hat{e}_f) \underline{I}_{i'j'}^{\text{loc}} \underline{R}(\hat{e}_f)^{-1} \underline{U}(\Delta\vec{R}_v)^{-1} , \quad (15)$$

where the 3×3 matrix D_{ij} represents the transformation of the polarization vector of the light from the local to the global frame of reference.

III. COMPUTATIONAL DETAILS

The electronic structure of the investigated ferromagnet bcc Fe, has been calculated self-consistently using the SPR-KKR band structure method^{40,41}. For the LSDA exchange-correlation potential the parametrization as given by Vosko et al.⁴² has been used and the experimental lattice parameter have been taken. For the angular momentum expansion within the KKR multiple-scattering method a cutoff of $l_{\text{max}} = 3$ was used. The temperature effects are treated within the alloy analogy scheme based on the CPA alloy theory. For the description of the magnetic spin fluctuations the temperature-dependent magnetization data were taken from experimental magnetization curves⁴³ and the lattice displacements as a function of temperature has been calculated using the Debye temperature of $T = 420$ K. In addition to the LSDA calculations, a charge and self-energy self-consistent LSDA+DMFT scheme for correlated systems based on the KKR approach^{44,45} has been used. The many-body effects are described by means of dynamical mean field theory (DMFT)⁴⁶ and the relativistic version of the so-called spin-polarized T-matrix fluctuation exchange approximation^{47,48} impurity solver was used. The realistic multiorbital interaction has been parametrized by the average screened Coulomb interaction U and the Hund exchange interaction J . In our calculations of bcc Fe we used values for the Coulomb parameter $U = 1.5$ eV and $J = 0.9$ eV as found by our previous ARPES studies on Fe^{49,50}.

In a second step the self consistent potential and DMFT self energy for bcc Fe has been used to calculate the photoemission response from the Fe(001) surface by means of the one step model of photoemission as presented above.

IV. RESULTS AND DISCUSSION

A. Temperature dependent ground state

First, let's discuss the impact of thermal lattice vibration and spin fluctuations on the ground state electronic structure of a magnetic solid, focusing on the temperature induced modification of the density of states (DOS). In an ordered material, the spin (s) resolved density of states is represented by the sum $n_s(E) = \frac{1}{N} \sum_{\vec{k}} \delta(E - E_s(\vec{k}))$, with $E_s(\vec{k})$ the energies of the electron states characterized by an infinite life time in the case of $T = 0$ K. On the other hand, at a finite temperature, $T > 0$ K, the electron scattering due to thermally induced lattice vibrations and spin fluctuations leads to a finite life time of the electronic states which can be accounted for within the KKR Green function formalism by giving the total DOS in terms of the Green function as follows

$$n(E) = -\frac{1}{\pi} \text{Im Trace } \underline{G}(E) . \quad (16)$$

Thermally induced lattice vibrations are treated here as random atomic displacements from the equilibrium positions, with the amplitude dependent on temperature. The same holds for the temperature induced tilting of the atomic spin moments. This creates a thermal disorder in the atomic positions and spin orientations having a similar impact on the electronic structure as chemical disorder in an alloy. In particular, it causes a broadening of the electronic states and a change of the exchange splitting of the states with opposite spin direction. Using the alloy analogy formalism described above, the Green function of the system, represented within multiple scattering theory is given in terms of the configurational average of the scattering path operator $\underline{\mathcal{I}}_{CPA}$ given by Eqs. (6) to (8).

As it will be shown below, spin fluctuations have a dominating contribution to the thermally induced modification of electronic structure when the temperature approaches the critical temperature T_C , where a transition to the paramagnetic (PM) state occurs. Thus, focusing on thermal spin fluctuations only, the scattering path operator averaged over spin fluctuations at a given temperature can be written as follows $\underline{\mathcal{I}}_{CPA} = \sum_f x_f \underline{\mathcal{I}}_f$, where $\underline{\mathcal{I}}_f$ is associated with the spin orientation \hat{e}_f , giving access to a corresponding DOS contribution $n_{f,s}(E)$. The DOS $n_{f,s}^{loc}(E)$ projected on spin s evaluated in the local frame of reference with $\hat{e}_{z'} = \hat{e}_f$ is different for different spin channels in the case of a non-zero local magnetic moment. This holds even for the PM (i.e. magnetically disordered) state with $\langle \hat{m} \rangle = 0$

in case of a non-vanishing local moment above T_C as it occurs, e.g. for bcc Fe. However, the average spin-projected DOS functions calculated for the PM state in a common global frame of reference are equal; i.e. one has $\langle n_{\uparrow} \rangle(E) = \langle n_{\downarrow} \rangle(E)$. Here, the indices \uparrow and \downarrow stand for a spin orientation along the global \hat{e}_z direction and opposite to it, respectively. Due to random orientation of the atomic spin magnetic moments in the system, the n_+ and n_- DOS projections are contributed equally by the electronic states characterized by different spin quantum numbers, implying mixed-spin character of the electronic states in such a system.

Fig. 1 (a) represents the DOS for bcc Fe calculated for the PM state ($\langle \hat{m} \rangle = 0$) in the local frame of reference (solid line), averaged over all possible orientations of the magnetic moment. This result is compared with the DOS at $T = 0K$. One can see first of all a finite exchange splitting of the majority and minority spin states at $T > T_C$. The main temperature effect is a significant broadening of the energy bands when compared to the case of $T = 0K$. However, in the global frame of reference the difference between the majority and minority-spin states decreases approaching the critical temperature $T_C = 1024K$. Above T_C , in the PM state, the difference vanishes between the DOS for different spin channels. However, this is not the case when only thermal lattice vibrations are taken into account (dashed line in Fig. 1 (a) for $T = 1025 K$). In this case only a weak broadening of the energy bands occurs, which is much weaker when compared to that due to spin fluctuations.

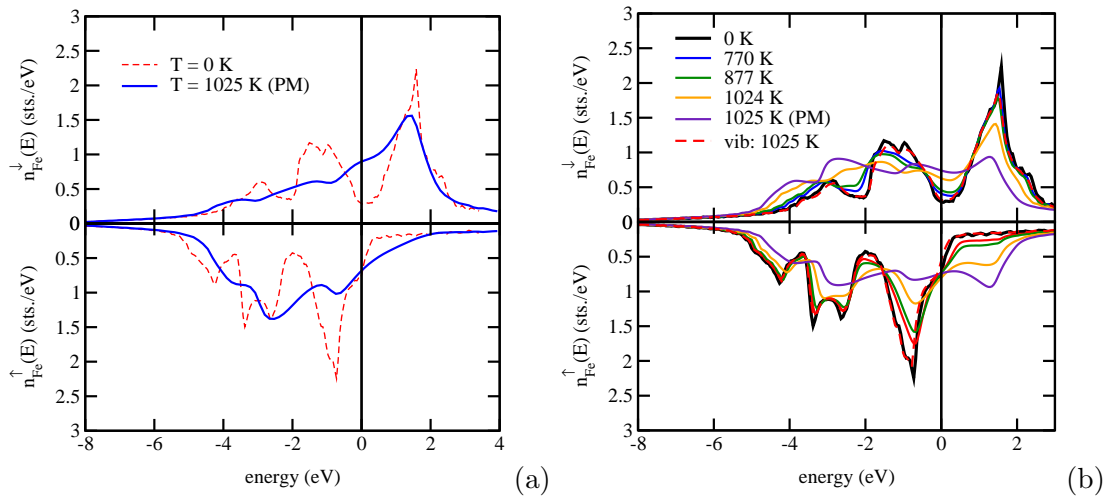


FIG. 1. Total spin resolved DOS for bcc Fe in the local (a) and the global (b) frames of reference.

B. Angle resolved photoemission of bcc Fe(001)

Although a large number of experimental spin-resolved ARPES studies on ferromagnetic transition metals are present in the literature, corresponding data for high temperatures are very rare. Experimental temperature-dependent studies have been carried out predominantly for Fe and Ni in the middle of 1980-ies (for review see Ref. 2). On the other hand, there have been several attempts to account for temperature-dependent ARPES within various different theoretical frameworks such as dynamical mean field theory¹⁸, or the disorder local moment approach⁵¹. However, most theoretical models were limited either to $T = 0$ K or to temperatures above the critical temperature T_C , and are based on the ground state electronic structure only. This way these approaches are ignoring matrix element, surface and final state effects. Therefore the question whether ARPES can distinguish between the different models describing finite temperature spin correlations, as the Stoner or Heisenberg model, is still open¹⁶. The alloy analogy model in combination with the one-step model of photoemission, presented in Sec. II, allows to describe all the mentioned effects on the same level of accuracy. As a first illustration of an application of this approach we discuss results for temperature-dependent spin-resolved ARPES on Fe(001) and compare the calculated spectra with corresponding experimental data stemming from Kisker et al.⁵.

In Fig. 2 we compare experimental and theoretical LSDA based spin-resolved photoemission data for three different temperatures, namely $T = 0, 300$ and 900 K respectively. The data for 0 K are seen as a reference obtained by using the standard one-step model of photoemission scheme. All spectra have been calculated for normal emission geometry assuming s-polarized light with 60 eV photon energy. Prior to these calculations we performed a photon energy scan (k_z -scan) in order to identify the k_z position in the Brillouin zone. Due to the LSDA approximation the final states are usually shifted somewhat in energy with respect to the experimental spectra. In the case of Fe the photon energy of 60 eV corresponds to emission from the Γ point. The spin-resolved spectra reveal three main transitions with bulk states as initial states: a minority peak close to the Fermi level and a majority peak at -2.4 eV binding energy having both T_{2g} symmetry. The majority peak at -0.9 eV binding energy has E_g symmetry. This transition should be suppressed by using s-polarized light due to the selection rules. However, as mentioned by Kisker et al.⁵ due to the finite acceptance angle of the analyzer this transition has nevertheless been

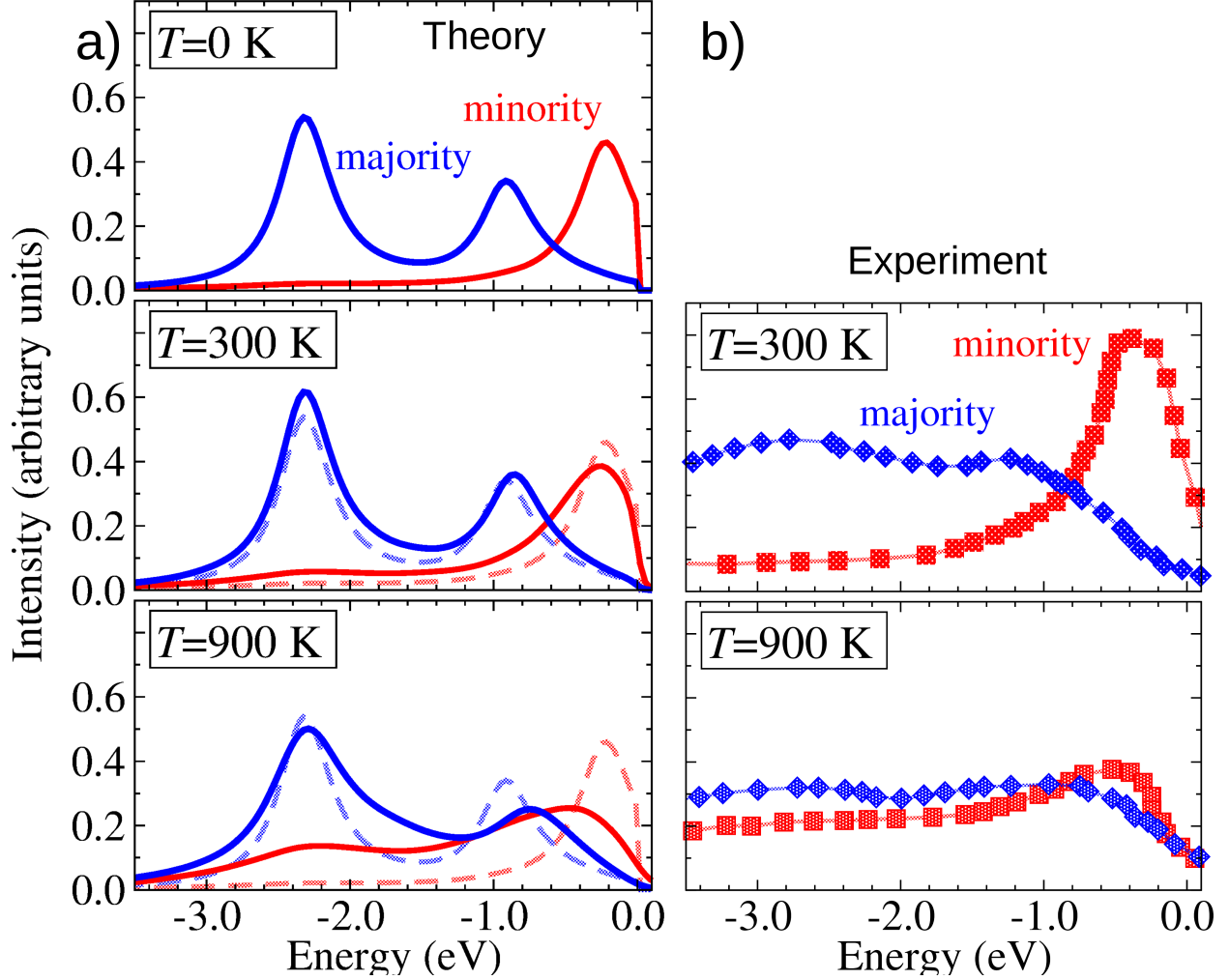


FIG. 2. Comparison between experimental (right panel) and theoretical LSDA based spectra (left panel) for temperature dependent spin resolved photoemission with at $E_{\text{phot}} = 60$ eV and normal emission. The dashed lines are spectra calculated for $T = 0$ K.

observed in the corresponding measurements. In addition a majority peak around -0.9 eV shows up with strong surface character and in fact it is a mixture of an E_g -like state and a surface d-like resonance. The minority surface states of Fe(001) close to the Fermi have been studied in detail in the past⁵² but could not be resolved in Kisker's work due to the limited experimental resolution.

In Fig. 2 (lower panel) results of finite temperature calculations (see Sec. II) are compared with corresponding experimental data. As a reference, calculated spectra for $T = 0$ K are given by dashed lines. Obviously, we obtained reasonable agreement with the experimental spectra. At $T = 900$ K the magnetization of Fe is decreased to roughly about 60% of

the value at $T = 300$ K. As one can see, at high temperature the E_g states are shifted towards the Fermi level. The exchange splitting of the T_{2g} states is reduced but still it remains considerably high. In particular, not only a reduction of the exchange splitting is observed but also an increase of the minority peak intensity at -2.5 and -0.9 eV is found in accordance with the experimental findings. This results from an increasing contribution from the majority spin states in line with the discussion in Sec. IV A. The overall reduction in the minority spin intensities at finite temperature is also a result of a varying contribution of the different spin channels to the 'spin-mixed' electronic states. In the calculations we can turn the lattice vibrations or spin fluctuations separately on and off. The main broadening effect in the spectra results from the spin fluctuations, while lattice vibrations have a minor effect on the spin polarization. However, as it was shown in the case of soft- and hard-X-ray photoemission²⁰ lattice vibrations will become more noticeable at higher photon energies.

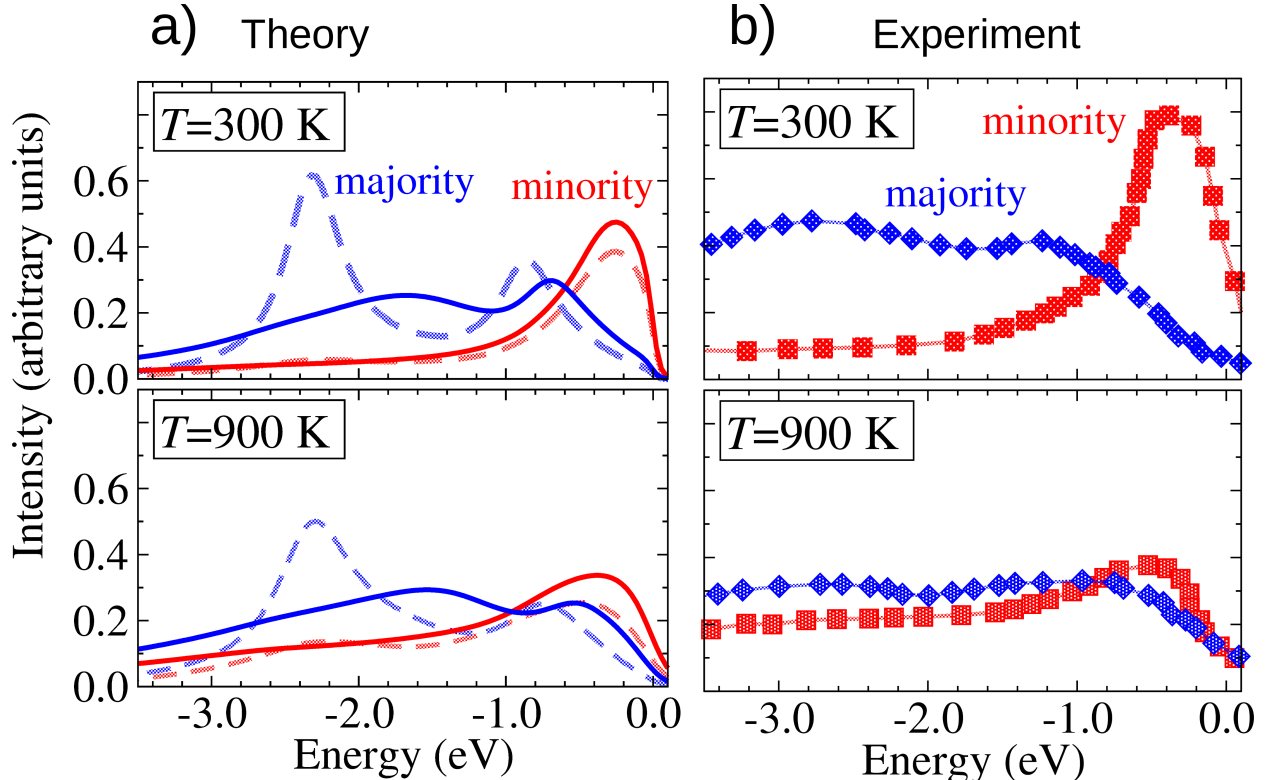


FIG. 3. Comparison between experimental (right panel) and theoretical LSDA+DMFT based calculations (left panel) for temperature dependent spin-resolved photoemission as measured for $E_{\text{phot}} = 60$ eV and normal emission. Dashed lines give calculated spectra obtained by means of LSDA (taken from Fig.2).

It can be seen from Fig. 2, that the overall agreement between the experimental data and the LSDA based calculations is quite reasonable. Also the temperature-dependency is well described by the LSDA calculations. However, LSDA based calculations underestimate the energy-dependent broadening and the position of the E_g peak is found at higher binding energy. One of the most successful approaches to include many-body effects beyond LSDA is the LSDA+DMFT scheme. Various aspects concerning a self-energy obtained via self-consistent LSDA+DMFT calculations for bcc-Fe have been discussed in detail recently in the context of ARPES^{49,50}. To find the best correspondence between the binding-energy positions and energy-dependent broadening of the theoretical peaks we have used for the averaged on-site Coulomb interaction U the value of $U = 1.5$ eV and exchange $J = 0.9$ eV. The chosen value for U lies between the estimated value $U \approx 1$ eV based on experiment⁵³ and the value $U \approx 2$ eV derived from theoretical studies^{54,55}. The most pronounced difference between LSDA+DMFT calculations and corresponding experimental results concerns the majority T_{2g} state which in the LSDA+DMFT calculations is shifted towards the Fermi level. On the other hand, the energetic position of this peak is better reproduced by plain LSDA calculations as shown in Fig. 2. These differences may indicate a strong influence of nonlocal correlations in the case of Fe^{49,50}.

In the following we address the question to which extent strongly correlated systems can be investigated by means of an implementation suited to deal with only moderately correlated systems. In general local spin fluctuations and corresponding correlations are formally included in the LSDA+DMFT calculations if a numerically exact DMFT impurity solver is used, e.g. by using the continuous time Monte Carlo method. On the other hand, the spin-polarized T-matrix fluctuation-exchange solver (SPTF)^{47,56} used to calculate the spectra presented in Fig. 3, has been implemented to treat the problem of magnetic fluctuations in transition metals, and has been successfully applied to the ferromagnetic phases of Fe, Co, Ni^{56–58} and to the anti-ferromagnetic phase of γ -Mn⁵⁹, as well as to half-metallic ferromagnets⁶⁰. This solver is quite stable, computationally rather cheap and deals with the complete four-indices interaction matrix. On the other hand, its perturbative character restricts its use to relatively weakly, or moderately, correlated systems. Not surprisingly, the SPTF performs well when starting from a spin-polarized solution, since the spin-splitting contains already the main part of the exchange and correlation effects. On the other hand, the direct application of SPTF to a non-magnetic reference state can create stability prob-

lems. This is because one tries to attribute the strong and essentially mean-field effect of the formation of a local magnetic moment to dynamical fluctuations around the non-spin-polarized state. Using a non-magnetic reference state causes no problems when one uses the quantum Monte Carlo (MC) method, which has no formal restrictions on the amplitude of fluctuations, but seems problematic for perturbative approaches. As a way to reduce the limitations for the latter case we propose a combination of SPTF with the disordered local moment approach^{61,62}. As already shown for the case of actinides⁶³ the inclusion of the fluctuations of randomly oriented local moments can improve drastically the description of the energetics in the paramagnetic phase. Therefore, as it is demonstrated in Fig. 3 one can hope that the combination of spin fluctuations treated within the alloy analogy model presented here in combination with a perturbative DMFT solver allows us to extend the range of applicability of SPTF.

Within the recent novel ultra fast pump-probe spin-resolved photoemission experiments on ferromagnetic materials¹⁶ time-dependent demagnetization is reflected by a corresponding change in the exchange splitting. Several mechanisms for this observation have been proposed in the literature. Among others, Eich et al. discussed as two possible limiting physical models the itinerant electron Stoner-like approach versus the localized electron Heisenberg spin-fluctuation picture. While the first model allows only for a homogeneous longitudinal magnetisation in the system, the later one accounts for transversal spin fluctuations as well. Referring to a common spin quantization axis in the system, these lead to a band mirroring, i.e. to a transfer of spectral weight of majority- or minority-spin states to mirrored states located close in binding energy but with opposite spin. Here we point out, that a point of view similar to the band mirroring picture has been introduced in a more formal way in the past when dealing with itinerant ferromagnets at finite temperatures^{61,64–66}. The approach leads to so-called shadow bands and was used among others to discuss the temperature dependence of ARPES as well as magnetoresistance measurements⁶⁴. Both of these models will lead to different signatures in the spin-resolved ARPES data and the main question is to what extent are these two models distinguishable by the use of ab-initio based calculated ARPES spectra. The formalism presented in this manuscript allows to model quantitatively and to predict in detail all possible differences in the corresponding ARPES spectra. In the left panel of Fig. 4 we summarize spin-resolved spectra for the Heisenberg model as calculated by the alloy analogy model for $T = 0, 300$ and 900 K (results taken

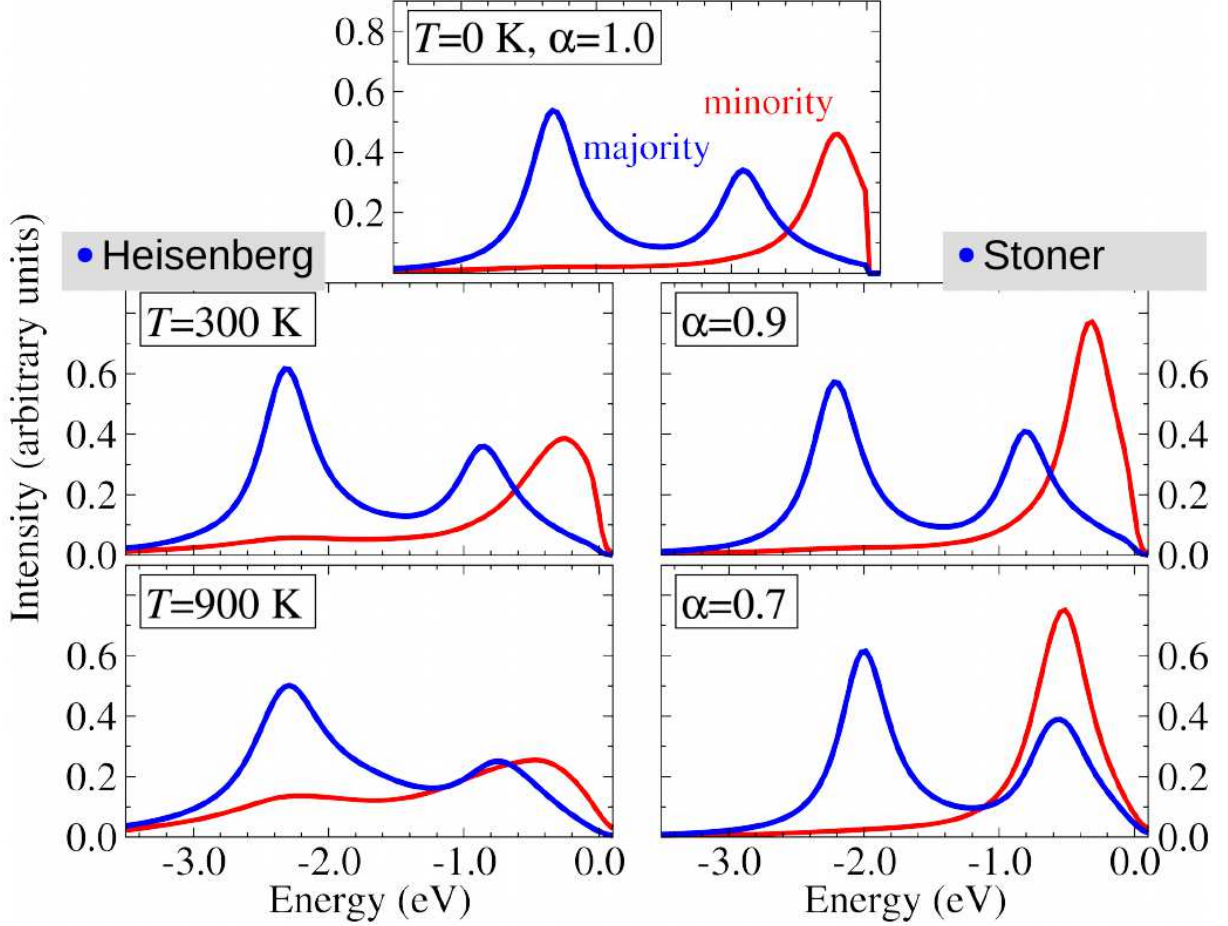


FIG. 4. Calculated spin resolved ARPES spectra for $E_{\text{phot}} = 60$ eV and normal geometry. The results in the top panel are calculated spectra for $T = 0$ K. Bottom left panel: calculated LSDA results based on the alloy analogy model (Heisenberg model). Bottom right panel: calculated LSDA results applying a modified exchange splitting (Stoner model).

from Fig. 2). In the right panel, we present calculated spectra for a modified exchange field $B(\vec{r}) = \alpha B(\vec{r})$, where α is a scaling factor which has been chosen in such a way that the local magnetic moment of Fe follows the experimental magnetization curve. We obtain significant differences between the two models. Within the Heisenberg model the minority-spin channel develops a second peak at higher binding energy, this way reflecting **the shadow bands and band mirroring picture**. Whereas, the Stoner model leads to a shift of the minority spin states towards higher binding energies. Finally, as shown in the Fig. 5, above T_C the Heisenberg picture still leads to a non-zero spin polarization in the spin-polarized ARPES

spectra due to the photoemission process. On the other hand, the Stoner model leads to zero spin polarization above T_C and the main intensity is found at a binding energy of about 1 eV. As a consequence one may state that these explicit spectroscopical calculations provide an adequate tool to distinguish between the various physical mechanisms involved.

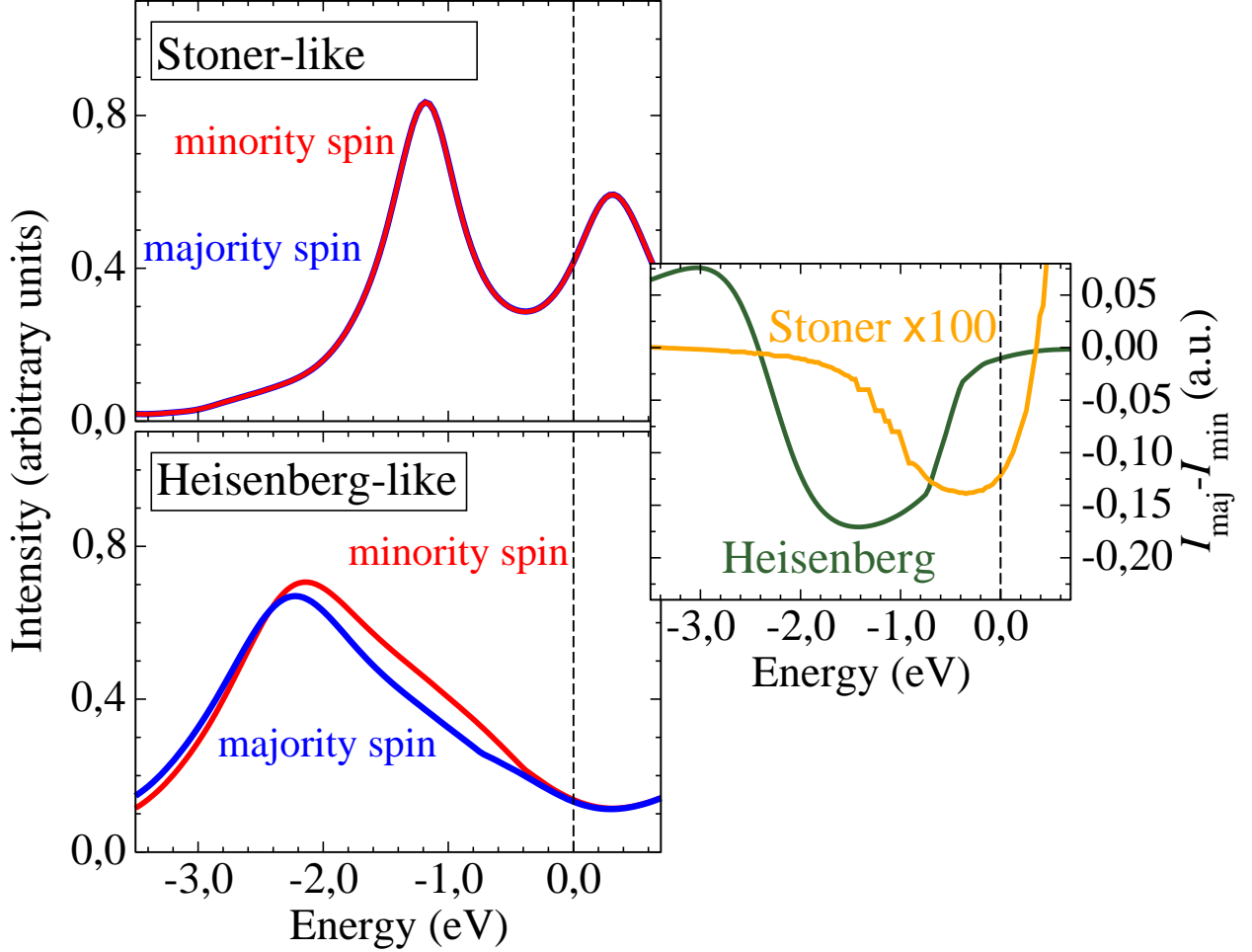


FIG. 5. Left panel: Comparison of spin resolved ARPES intensities between Stoner- and Heisenberg-like model calculated at $T = 1100$ K close to ferro- to paramagnetic transition. Right panel: Corresponding spin difference $I_{maj} - I_{min}$.

V. CONCLUSIONS

We have introduced a generalization of the one-step model of photoemission for finite temperatures. The scheme is based on the alloy analogy model that allows for the inclusion of thermal effects when calculating spin-resolved ARPES spectra. The technical details of

the implementation using the spin-polarized relativistic coherent potential approximation within the one-step model of photoemission have been outlined. This formalism allows to deal quantitatively with spin-fluctuations as well as with lattice vibrations on the same footing. In the present contribution we have discussed temperature-dependent, spin-resolved ARPES spectra of Fe(001). Our calculated photoemission spectra for Fe(001) were found to match quantitatively the experimental data. To overcome the limitations of local density approximation based calculations applications of the LSDA+DMFT scheme have been presented and discussed. The inclusion of electronic correlations described by the perturbative SPTF-DMFT many body solver in combination with randomly fluctuating local moments improve the description of the corresponding spectra in the paramagnetic phase.

As it was shown, the alloy analogy model can be used to describe and predict changes of the spin-polarized spectra due to the ultrafast processes obtained in pump-probe photoemission. Here we showed that the Heisenberg like **band mirroring mechanism which leads to the shadow bands** provide an adequate model to describe recent experimental findings.

VI. ACKNOWLEDGEMENTS

Financial support by DFG (Ebe154/32-1) is thankfully acknowledged. J.M. would like to thank CEDAMNF project financed by Ministry of Education, Youth, and Sports of Czech Rep., Project No. CZ.02.1.01/0.0/0.0/15_003/0000358. Authors would like to thank Voicu Popescu for the discussions and his support when preparing some graphs.

* jminar@ntc.zcu.cz

¹ Dieter Vollhardt, N Blümer, K Held, M Kollar, J Schlipf, M Ulmke, and J Wahle, *Advances in Solid State Physics* **38** (Springer, ADDRESS, 1999), pp. 383–396.

² Peter D Johnson, *Reports on Progress in Physics* **60**, 1217 (1997).

³ J Hugo Dil, *Electronic Structure* **1**, 023001 (2019).

⁴ E Kisker, *Journal of magnetism and magnetic materials* **45**, 23 (1984).

⁵ E Kisker, K Schröder, W Gudat, and M Campagna, *Physical Review B* **31**, 329 (1985).

⁶ E Kisker, K Schröder, M Campagna, and W Gudat, *Physical review letters* **52**, 2285 (1984).

- ⁷ Andrea Damascelli, Zahid Hussain, and Zhi-Xun Shen, *Rev. Mod. Phys.* **75**, 473 (2003).
- ⁸ Jrgen Braun, Jn Minr, and Hubert Ebert, *Physics Reports* **740**, 134 (2018), correlation, temperature and disorder: Recent developments in the one-step description of angle-resolved photoemission.
- ⁹ Joseph C Woicik and Joseph Woicik, *Hard X-ray photoelectron spectroscopy (HAXPES)* (Springer, ADDRESS, 2016), Vol. 59.
- ¹⁰ Charles S Fadley, *Synchrotron Radiation News* **25**, 26 (2012).
- ¹¹ A. X. Gray, C. Papp, S. Ueda, B. Balke, Y. Yamashita, L. Plucinski, J. Minár, J. Braun, E. R. Ylvisaker, C. M. Schneider, W. E. Pickett, H. Ebert, K. Kobayashi, and C. S. Fadley, *Nature Materials* **10**, 759 (2011).
- ¹² F. Venturini, J. Minár, J. Braun, H. Ebert, and N. B. Brookes, *Phys. Rev. B* **77**, 045126 (2008).
- ¹³ L. Plucinski, J. Minár, B. C. Sell, J. Braun, H. Ebert, C. M. Schneider, and C. S. Fadley, *Phys. Rev. B* **78**, 035108 (2008).
- ¹⁴ J. Minár, J. Braun, and H. Ebert, *J. Electron. Spectrosc. Relat. Phenom.* **190**, 159 (2013).
- ¹⁵ C. Cacho, A. Crepaldi, M. Battiato, J. Braun, F. Cilento, M. Zacchigna, C. Richter, M. O. Heckmann, E. Springate, Y. Liu, S. Dhesi, S. H. Berger, Ph. Bugnon, K. Held, M. Grioni, H. Ebert, K. Hricovini, J. Minár, and F. Parmigiani, *Phys. Rev. Lett.* **114**, 097401 (2015).
- ¹⁶ Steffen Eich, Moritz Plötzing, Markus Rollinger, Sebastian Emmerich, Roman Adam, Cong Chen, Henry Cornelius Kapteyn, Margaret M. Murnane, Lukasz Plucinski, Daniel Steil, Benjamin Stadtmüller, Mirko Cinchetti, Martin Aeschlimann, Claus M. Schneider, and Stefan Mathias, *Science Advances* **3**, (2017).
- ¹⁷ A I Liechtenstein, M I Katsnelson, V P Antropov, and V A Gubanov, *J. Magn. Magn. Materials* **67**, 65 (1987).
- ¹⁸ A. I. Lichtenstein, M. I. Katsnelson, and G. Kotliar, *Phys. Rev. Lett.* **87**, 067205 (2001).
- ¹⁹ H. Ebert, S. Mankovsky, D. Ködderitzsch, and P. J. Kelly, *Phys. Rev. Lett.* **107**, 066603 (2011).
- ²⁰ J. Braun, J. Minár, S. Mankovsky, V. N. Strocov, N. B. Brookes, L. Plucinski, C. M. Schneider, C. S. Fadley, and H. Ebert, *Phys. Rev. B* **88**, 205409 (2013).
- ²¹ H. Ebert, S. Mankovsky, K. Chadova, S. Polesya, J. Minár, and D. Ködderitzsch, *Phys. Rev. B* **91**, 165132 (2015).
- ²² J Staunton, B L Gyorffy, A J Pindor, G M Stocks, and H Winter, *J. Magn. Magn. Materials* **45**, 15 (1984).

- ²³ J. B. Staunton, M. Banerjee, dos Santos Dias, A. Deak, and L. Szunyogh, Phys. Rev. B **89**, 054427 (2014).
- ²⁴ K. Chadova, S. Mankovsky, J. Minár, and H. Ebert, Phys. Rev. B **95**, 125109 (2017).
- ²⁵ J B Pendry, Surf. Sci. **57**, 679 (1976).
- ²⁶ J F L Hopkinson, J B Pendry, and D J Titterington, Comp. Phys. Commun. **19**, 69 (1980).
- ²⁷ J. Minár, J. Braun, S. Mankovsky, and H. Ebert, J. Electron. Spectrosc. Relat. Phenom. **184**, 91 (2011).
- ²⁸ J. Minár, J. Braun, and H. Ebert, J. Electron. Spectrosc. Relat. Phenom. **189**, 129 (2013).
- ²⁹ N. Papanikolaou, R. Zeller, P. H. Dederichs, and N. Stefanou, Phys. Rev. B **55**, 4157 (1997).
- ³⁰ A Lodder, J. Phys. F: Met. Phys. **6**, 1885 (1976).
- ³¹ M E Rose, *Relativistic Electron Theory* (Wiley, New York, 1961).
- ³² S Tikadzumi, in *Physics of Magnetism* (Wiley, New York, 1964).
- ³³ J. S. Faulkner and G. M. Stocks, Phys. Rev. B **21**, 3222 (1980).
- ³⁴ J Braun, Rep. Prog. Phys. **59**, 1267 (1996).
- ³⁵ P J Durham, W M Temmerman, C G Larsson, and P O Nilsson, Vacuum **33**, 771 (1983).
- ³⁶ J. Braun, J. Minár, F. Matthes, C. M. Schneider, and H. Ebert, Phys. Rev. B **82**, 024411 (2010).
- ³⁷ B Ginatempo, P J Durham, and B I Gyorffy, J. Phys.: Cond. Mat. **1**, 6483 (1989).
- ³⁸ P J Durham, J. Phys. F: Met. Phys. **11**, 2475 (1981).
- ³⁹ A I Liechtenstein, M I Katsnelson, and V A Gubanov, J. Phys. F: Met. Phys. **14**, L125 (1984).
- ⁴⁰ H. Ebert et al., *The Munich SPR-KKR package*, version 7.7, <http://olymp.cup.uni-muenchen.de/ak/ebert/SPRKKR>, 2017.
- ⁴¹ H Ebert, D Ködderitzsch, and J Minár, Rep. Prog. Phys. **74**, 096501 (2011).
- ⁴² S H Vosko, L Wilk, and M Nusair, Can. J. Phys. **58**, 1200 (1980).
- ⁴³ J. Crangle and G. M. Goodman, Proc. Roy. Soc. (London) A **321**, 477 (1971).
- ⁴⁴ J Minár, J. Phys.: Cond. Mat. **23**, 253201 (2011).
- ⁴⁵ J Minár, L Chioncel, A Perlov, H Ebert, M I Katsnelson, and A I Lichtenstein, Phys. Rev. B **72**, 045125 (2005).
- ⁴⁶ K Held, Adv. Phys. **56**, 829 (2007).
- ⁴⁷ L. V. Pourovskii, M. I. Katsnelson, and A. I. Lichtenstein, Phys. Rev. B **72**, 115106 (2005).
- ⁴⁸ I. Di Marco, J. Minár, S. Chadov, M. I. Katsnelson, H. Ebert, and A. I. Lichtenstein, Phys. Rev. B **79**, 115111 (2009).

- ⁴⁹ J. Sánchez-Barriga, J. Fink, V. Boni, I. Di Marco, J. Braun, J. Minár, A. Varykhalov, O. Rader, V. Bellini, F. Manghi, H. Ebert, M. I. Katsnelson, A. I. Lichtenstein, O. Eriksson, W. Eberhardt, and H. A. Dürr, *Phys. Rev. Lett.* **103**, 267203 (2009).
- ⁵⁰ J. Sánchez-Barriga, J. Braun, J. Minár, I. Di Marco, A. Varykhalov, O. Rader, V. Boni, V. Bellini, F. Manghi, H. Ebert, M. I. Katsnelson, A. I. Lichtenstein, O. Eriksson, W. Eberhardt, H. A. Dürr, and J. Fink, *Phys. Rev. B* **85**, 205109 (2012).
- ⁵¹ P J Durham, J Staunton, and B L Gyorffy, *J. Magn. Magn. Materials* **45**, 38 (1984).
- ⁵² L Plucinski, Yuan Zhao, CM Schneider, B Sinkovic, and E Vescovo, *Physical Review B* **80**, 184430 (2009).
- ⁵³ M. M. Steiner, R. C. Albers, and L. J. Sham, *Phys. Rev. B* **45**, 13272 (1992).
- ⁵⁴ Matteo Cococcioni and Stefano de Gironcoli, *Phys. Rev. B* **71**, 035105 (2005).
- ⁵⁵ S. Chadov, J. Minár, M. I. Katsnelson, H. Ebert, D. Ködderitzsch, and A. I. Lichtenstein, *Europhys. Lett.* **82**, 37001 (2008).
- ⁵⁶ M I Katsnelson and A I Lichtenstein, *European Physics Journal B* **30**, 9 (2002).
- ⁵⁷ J. Braun, J. Minár, H. Ebert, M. I. Katsnelson, and A. I. Lichtenstein, *Phys. Rev. Lett.* **97**, 227601 (2006).
- ⁵⁸ Alexei Grechnev, I. Di Marco, M. I. Katsnelson, A. I. Lichtenstein, John Wills, and Olle Eriksson, *Phys. Rev. B* **76**, 035107 (2007).
- ⁵⁹ I Di Marco, J Minár, J Braun, M I Katsnelson, A Grechnev, H Ebert, A I Lichtenstein, and O Eriksson, *Eur. Phys. J. B* **72**, 473 (2009).
- ⁶⁰ M. I. Katsnelson, V. Yu. Irkhin, L. Chioncel, A. I. Lichtenstein, and R. A. de Groot, *Rev. Mod. Phys.* **80**, 315 (2008).
- ⁶¹ B L Gyorffy, A J Pindor, J Staunton, G M Stocks, and H Winter, *J. Phys. F: Met. Phys.* **15**, 1337 (1985).
- ⁶² J B Staunton, *Rep. Prog. Phys.* **57**, 1289 (1994).
- ⁶³ Anders MN Niklasson, John M Wills, Mikhail I Katsnelson, Igor A Abrikosov, Olle Eriksson, and Börje Johansson, *Physical Review B* **67**, 235105 (2003).
- ⁶⁴ A. H. MacDonald, T. Jungwirth, and M. Kasner, *Phys. Rev. Lett.* **81**, 705 (1998).
- ⁶⁵ V. Korenman, J. L. Murray, and R. E. Prange, *Phys. Rev. B* **16**, 4032 (1977).
- ⁶⁶ H Capellmann, *Journal of Physics F: Metal Physics* **4**, 1466 (1974).